

Machine learning many-body localization: Search for the elusive nonergodic metal

Yi-Ting Hsu,^{1,*} Xiao Li,^{1,†} Dong-Ling Deng,^{1,2} and S. Das Sarma¹

¹*Condensed Matter Theory Center and Joint Quantum Institute,
University of Maryland, College Park, MD 20742, USA*

²*Institute for Interdisciplinary Information Sciences, Tsinghua University, Beijing, China, 100084*

(Dated: August 5, 2019)

The many-body localization transition in isolated quantum systems with a single-particle mobility edge is an intriguing subject that has not yet been fully understood. In particular, whether a nonergodic metallic phase associated with a many-body mobility edge exists or not is under active debate. In this Letter, we construct a neural network classifier to investigate the existence of the nonergodic metallic phase in a prototype model using many-body entanglement spectra as the sole diagnostic. We find that such a classifier is able to identify with high confidence the nonergodic metallic phase existing between the many-body localized and the thermal phase. Our neural network based approach shows how supervised machine learning can be applied not only in locating phase boundaries, but also in providing a way to definitively examine the existence of a novel phase whose existence is unclear.

Introduction— Investigating the energy-resolved properties of eigenstates in isolated quantum many-body systems is essential for understanding dynamical phases and their transitions, and even more importantly, the very question of thermal equilibrium in quantum statistical mechanics. In the noninteracting limit, the single-particle orbitals of a fermionic system throughout the spectrum can be all localized [1], all extended, or exhibit a single-particle mobility edge (SPME) [2–12] separating localized and extended states. The SPME is in fact thought to be the generic situation for three-dimensional disordered systems. Moreover, the existence of an SPME in an incommensurate one-dimensional (1D) system has been predicted and experimentally observed in a quasiperiodic optical lattice [13, 14].

In the presence of interaction, we can further introduce the notion of ergodicity for a many-body eigenstate since a closed quantum system can thermalize according to the eigenstate thermalization hypothesis (ETH) [15, 16]. Since the critical energies for the localization and thermalization transitions do not necessarily coincide, more complicated eigenstate phases can occur other than all eigenstates throughout the many-body spectrum being many-body localized (MBL) [17–39], i.e. localized and nonergodic, or all obey ETH, i.e. extended and ergodic. In particular, recent numerical studies have found that in systems subject to a family of incommensurate potentials that exhibit SPME, there exists a finite energy window wherein the eigenstates are nonergodic but extended [32–34]. Such an intriguing eigenstate phase was subsequently named the *nonergodic metal* (NEM) [33]. Note that the existence of NEM is necessarily connected with the existence of a many-body mobility edge (MBME) in the corresponding many-body energy spectrum, the idea being that the noninteracting SPME may evolve to an MBME in the presence of interaction. Whether such an MBME, and consequently the NEM phase, exists or not has remained controversial.

The common strategy taken by prior studies on MBME [28–39] was to detect localization and ergodicity by different diagnostics. This was necessary since different phases are naturally more sensitive to different diagnostics, which is also true in the experimental studies of MBL [40–43]. The problem with this strategy is that these *ad hoc* different diagnostics may not necessarily be equivalent with respect to their sensitivity to various phases. For instance, while entanglement entropy and local particle number fluctuations were used to diagnose localization and ergodicity in Ref. [33], the inverse participation ratio and the return probability were used in Ref. [32] along with several other diagnostics. Since the energy window for NEM is set by the two transition energies corresponding to the two diagnostics respectively, the phase space or even the existence of NEM itself can largely depend on the combination of the diagnostics used, which is unsatisfactory. Thus it is highly desirable to develop a universal approach to distinguish MBL, NEM, and the extended thermal (ET) phase based on a single diagnostic.

Entanglement spectrum (ES) [44] is an appealing choice in this context because of the following reasons. First, an ES contains more information about the eigenstates than entanglement entropy due to the lack of the tracing procedure. Second, recent studies have indicated ES as a sensitive probe for MBL and ET phases [45–48]. Yet, the complexity of the spectral pattern in ES makes it generally difficult to extract the relevant features necessary for discerning eigenstate properties.

Machine learning has recently been introduced to condensed matter physics, raising tremendous interest in the community [49–66]. In particular, supervised machine learning has been used as a successful numerical tool to study phases and their transitions [49–52]. One application is to identify the phase boundaries throughout the parameter space using a neural network (NN) classifier trained with data obtained from well-known limits deep

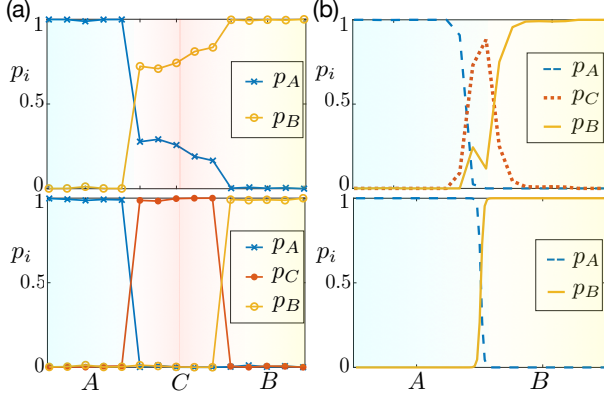


FIG. 1. Schematic results produced by different classifiers for studying systems with (a) three phases A, B, and C, and (b) two phases A and B. The outputs p_i of a classifier are the confidence the network has for identifying certain input data as phase i . In (a), the upper panel shows the falsely negative result produced by a two-phase classifier for only A and B. The lower panel shows the correct result produced by a three-phase classifier for A, B, and C. The plots in (a) are produced by using MNIST data as input, where we associate A, B, and C with digit 1, 6, and 3, respectively. The ranges on the horizontal axis with background color blue, red, and yellow correspond to phase A, C, and B, respectively. Each tick on the horizontal axis corresponds to a group of 160 MNIST images of the associated digit. In (b), the upper panel shows the falsely positive result produced by a three-phase classifier for A, B, and C. The lower panel shows the correct result produced by a two-phase classifier for A and B. The plots in (b) are schematics to illustrate situations described in the text.

in each phase [46, 49, 67, 68]. Such an approach, however, relies on the prior knowledge of how many phases there are throughout the parameter space, which is not always available. To the best of our knowledge, studies in this direction have so far been limited to models where the existence of all the phases are well established without controversies.

In this Letter, we apply supervised machine learning for a rather different purpose—as a useful tool for examining the existence of a controversial phase in MBL physics. Using this novel approach, we investigate whether the NEM phase exists or not in a prototype incommensurate 1D lattice model [33]. Using ES as the input data, we show that a three-layer NN is able to uniquely (and unambiguously) identify a distinct new phase between MBL and ET phases with a high confidence. Our results provide the strongest numerical evidence so far for the existence of NEM, and also usher in a machine learning based new technique for identifying novel phases of matter.

The NN approach— Our approach establishes guidelines for building different NN-classifiers according to the candidate phase diagrams we have in mind, and telling from the outputs of these classifiers whether the number

of phases we assume is correct. The technique is powerful enough to eliminate both false negatives (not identifying an existing phase) and false positives (incorrectly identifying a non-existing phase). We first demonstrate such guidelines using a toy example, where we associate each ‘phase’ with a set of images of a hand-written digit from the MNIST database [69], a canonical source of input datasets for benchmarking machine learning algorithms. To better connect to the MBL phase diagram of interest in this work, we present the results of this example by ‘phase diagrams’ consisting of different digits. To mimic the continuous tuning parameter in usual phase diagrams, we divide the testing data for each digit into groups and plot the output of the network against the group label.

First imagine a situation where we only know of phases A and B, but are not sure if some phase C exists between them. To investigate the existence of C, we can build a two-phase classifier trained by data from small phase spaces in A and B, and use it to produce the complete phase diagram. If there is indeed a hidden phase C, we expect to see a wide phase space between A and B where the network shows low confidence p_i ($i = A, B$) in deciding whether C resembles A or B more [top panel of Fig 1(a)]. Such a false negative result is in contrast to the phase diagram in the bottom panel in Fig 1(a), which is produced by a three-phase classifier trained by data from A, B, and C. Here the transition regimes are much narrower, and each phase consists of a wide phase space with a nearly perfect network confidence.

Now imagine the opposite situation where the studied phase space actually contains only phases A and B, but we build a three-phase classifier trained by data chosen from small regimes within the phase spaces of A, B, and within a phase space we thought to be C but is actually a part of B. Two scenarios can happen in this case. First, for simpler phases with low variance within each phase, the training procedure itself would fail with a low accuracy. Our example based on MNIST data falls in this category. Second, for more complicated phases with higher variance within each phase, the training process could have a high accuracy but the regime identified as phase C with a high confidence would be negligible or (at best) similar in size to the small regime where the training data for C were collected. This is because instead of capturing universal properties of a phase, the network is actually trained to capture detailed features tied to just the small phase spaces used for training. We show a schematic in the upper panel of Fig. 1(b) illustrating such a situation, where the confusion between phases B and C suggests fewer phases in reality than we assumed at the outset and therefore necessitates further investigations. This is in contrast to the phase diagram [lower panel in Fig. 1(b)] produced by a two-phase classifier for A and B that matches the reality.

Model and method— Motivated by the results shown

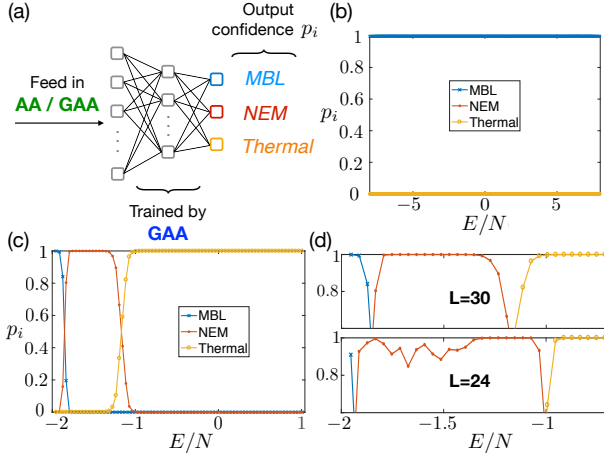


FIG. 2. (a) The schematics for the three-phase classifier for the MBL, NEM, and thermal phases we benchmark against the AA model. The resulting phase diagrams of the AA model with potential strength (b) $\lambda = 4.0$ and (c)-(d) $\lambda = 0.3$, where $p_i(E)$, $i = 1, 2, 3$ are the energy-dependent confidence at which the three-phase classifier identifies the eigenstates to be in the MBL, NEM, and thermal phases, respectively. The plots in (b) and (c) are for the $L = 24$ and $L = 30$ case, respectively. (d) shows the comparison between the $L = 30$ (upper) and $L = 24$ (lower) diagrams zoomed in on the NEM regimes. Here we choose the interaction strength $V = 1$.

in Fig. 1, we now apply the NN approach to study two models for spinless fermions subject to incommensurate potentials in a 1D system of size L with a particle number of $N = L/6$: the generalized Aubry-Andre (GAA) model [12], whose MBL phase diagram was recently reported to contain an NEM regime [33], and the original Aubry-Andre (AA) model [70], whose many-body spectrum is well-known to contain only the MBL or ET phase [23, 40–42]. The GAA model $H = H_0 + H_{int}$ has the form [33]

$$H_0 = \sum_{j=1}^L \left[-t(c_j^\dagger c_{j+1} + H.c.) + 2\lambda \frac{\cos(2\pi q j + \phi)}{1 - \alpha \cos(2\pi q j + \phi)} n_j \right],$$

$$H_{int} = V \sum_{j=1}^L n_{j+1} n_j, \quad (1)$$

where $n_j = c_j^\dagger c_j$ is the fermionic number operator at site j , V is the nearest-neighbor interaction strength, and t denotes the nearest-neighbor hopping strength. We use t as the energy unit throughout the article. The second term in H_0 describes an incommensurate potential with strength 2λ , an irrational wave number $q = 2/(1 + \sqrt{5})$, a randomly chosen global phase ϕ , and a dimensionless parameter $\alpha \in (-1, 1)$. The $\alpha = 0$ case corresponds to the pristine AA model [70], where single-particle orbitals are all localized or extended for $\lambda > 1$ and $\lambda < 1$, respectively (i.e. no SPME) in the noninteracting limit $V = 0$. As for the general $\alpha \neq 0$ case, SPME exists for finite win-

dows in λ and α . In this study, we choose $\lambda = 0.3$ and $\alpha = -0.8$ so that the single-particle spectrum consists of a comparable number of localized and extended orbitals in the noninteracting limit [33]. This choice ensures that no accidental domination by either localized or extended states can happen when the interaction is turned on.

With interaction $V \neq 0$, in the AA model limit the many-body spectrum is numerically shown to contain only MBL or ET states [23]. In fact, the existence of MBL in the interacting AA model has been experimentally demonstrated in optical lattices [40–42]. For the GAA model, however, the interacting many-body spectrum at some fixed λ may contain a finite energy window $E_L < E < E_T$ with nonergodic but extended eigenstates (i.e. NEM) if we diagnose localization and ergodicity by the scaling of entanglement entropy and local density fluctuation, respectively [33]. Meanwhile, MBL and ET phases are expected for $E < E_L$ and $E > E_T$, respectively. The important question we are studying in the current work using NN classifiers is the existence of the NEM phase in the interacting GAA model in the intermediate energy window.

To generate the input ES data for the NN classifier, we first divide the entire system into two subsystems \mathcal{A} and \mathcal{B} of equal sizes ($L/2$). For each many-body eigenstate $|\psi\rangle$ (obtained by exact diagonalization methods), we calculate its reduced density matrix $\rho_{\mathcal{A}} = \text{tr}_{\mathcal{B}} |\psi\rangle \langle \psi|$ and then obtain the ES, which is the spectrum of $\rho_{\mathcal{A}}$. The input data are generated by randomly assigning the global phase ϕ while keeping the other parameters fixed. These data are then sorted into a series of energy bins with a width of $0.04t$, which constitute the unit of energy throughout the rest of this paper. We have checked that the size of these energy bins is sufficiently small for ensuring convergence of our numerics.

In the following we describe how we build the three-phase classifier distinguishing MBL, NEM, and ET phases. The network structure of the classifier contains an input layer, a hidden layer, and an output layer [see Fig. 2(a)]. The size of the input layer is determined by the size of the input ES data, and the hidden layer contains 30 sigmoid neurons. The output layer contains three softmax neurons, and each produces a real number $p_i \in [0, 1]$, $i = 1, 2, 3$, with $\sum_{i=1}^3 p_i = 1$. Thus, the three outputs can be viewed as the confidence the classifier identifies the input ES as belonging to MBL, NEM, and ET phase, respectively. During the training process, we feed the training data to the input layer and allow the all-to-all couplings between the adjacent layers to evolve from randomly chosen initial values according to the log-likelihood cost function. The training data set is generated from the three energy bins labeled by E_1 , E_2 , and E_3 in Fig. 3(a), which are chosen according to the phase diagram in Ref. [33]. We then test the trained network with another independent set of testing data obtained in the same way. If the training is successful, which we de-

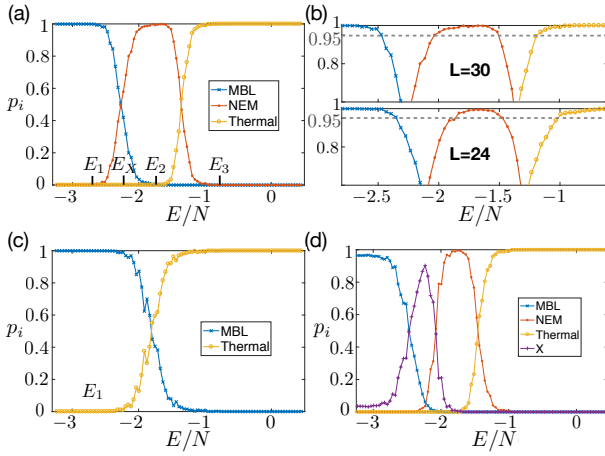


FIG. 3. The phase diagrams of the GAA model with potential strength $\lambda = 0.3$ produced by (a)-(b) the three-phase classifier, (c) the two-phase classifier, and the (d) four-phase classifier. Here $p_i(E)$ are the energy-dependent confidence at which the corresponding classifier identifies the eigenstates to be in each of the studied phases. (a) shows the full diagram for the $L = 30$ case, and (b) shows the comparison between the $L = 30$ (upper) and $L = 24$ (lower) diagrams zoomed in on the NEM regimes. The plot in (c) and (d) are both for the $L = 30$ case. Here we choose the interaction strength $V = 1$.

fine as obtaining a testing accuracy over 99%, we feed the trained network with ES from all energy bins throughout the spectrum in order to obtain the energy-resolved confidence $p_i(E)$, $i = 1, 2, 3$.

Results— To test the reliability of our approach, we first demonstrate that the phase diagrams for the $\alpha=0$ case generated by the three-phase classifier qualitatively reproduce results expected for the AA model in a finite-size system. The many-body spectra of AA model under strong ($\lambda=4.0$) and weak ‘disorder’ potential ($\lambda=0.3$) are expected to contain only MBL and only ET eigenstates respectively [23]. For a finite-size system, however, we expect the edge of the energy spectra to be more sensitive to the finite-size effect than the mid-spectra, thus reflecting some spurious nonergodicity.

For $\lambda = 4.0$, we find that the classifier identifies the eigenstates to be MBL throughout the full energy spectrum, which is consistent with the thermodynamic-limit expectations for the interacting AA model [see Fig. 2(b)]. Moreover, the confidence stays over 99.6% throughout the spectrum already at a smaller system size $L = 24$. As for the $\lambda = 0.3$ case [see Fig. 2(c)], we find that in a larger system ($L = 30$) the classifier identifies eigenstates from most part of the spectrum as thermal and those from a small regime near the spectrum edges as non-thermal. While a non-thermal regime near the spectral edge is consistent with the input data suffering finite-size effects, we explicitly examine such an explanation by performing the same calculation in a smaller system ($L = 24$) and focus-

ing on how the width of the non-thermal regime change as L increases. We find that the non-thermal regime shrinks by nearly 40% as the system size increases from $L = 24$ to $L = 30$ [see Fig. 2(d)]. This finding supports the finite size explanation for the spectral edge states.

Having benchmarked our three-phase classifier against the AA model, we now employ it to study the phase diagram of the GAA model in a system with $L = 30$ with a fixed potential strength $\lambda = 0.3$ and interaction strength $V = 1$. We find that the classifier recognizes three types of eigenstate phases in different parts of the many-body spectrum [see Fig. 3(a)]. In particular, the classifier identifies the eigenstates as MBL, NEM, and ET phases with a high confidence as energy increases from the edge to the middle of the spectrum, which qualitatively agrees with the phase diagram found before using two diagnostics [33]. Our results give strong evidence for the existence of NEM under the lens of the single diagnostic ES in the finite-size system we study since (i) the training process is successful with a testing accuracy over 99%, and (ii) the width of the identified NEM regime (with over 95% confidence) is seven times wider than the size of the energy bin that was used to produce the training data for the NEM phase.

To further examine the existence of NEM under finite-size effect, we perform the same calculation for the $L = 24$ case by the same classifier that generates the AA model result in Fig. 2(b). We find that the regime identified as NEM with over 95% confidence increases by 40% as the system size increases from $L = 24$ to $L = 30$ [see Fig. 3(b)]. Moreover, for the $L = 18$ case we fail to even achieve a successful training process under a reasonable hyper-parameter scan. The above observations are both consistent with the NEM regime staying finite in the thermodynamic regime. Studying any system size $L > 30$ is not feasible under our current supercomputer resources. It is therefore extremely unlikely that our unbiased identification of the NEM phase as distinct from MBL/ET phases can be a finite size artifact.

The final step is to investigate more carefully whether the GAA phase diagram found by our three-phase classifier could be falsely positive or negative. To do so, we apply the same NN-based approach to study two other scenarios that could in principle happen: (i) the many-body spectrum consists of only MBL states near the edge of the energy spectrum and ET states in the middle but no NEM exists, and (ii) there exists another (unknown) intermediate phase X between, for instance, MBL and NEM phases. To examine the first scenario, we build a two-phase classifier with training and testing data from only energies deep in MBL (E_1) and ET (E_3) phases, respectively. We find that although the phase diagram produced by this two-phase classifier [see Fig. 3(c)] shows a smooth transition between MBL and ET phases, the transition becomes much wider than those in the result trained by the three-phase classifier [see Fig. 3(a)]. Such

a result suggests a possible hidden phase between MBL and ET phases, which is already confirmed by the results of the three-phase classifier.

For the second scenario, we show that it is not possible to obtain new intermediate phases following the same approach by assuming a fourth phase X between MBL and NEM phases. Using a four-phase classifier trained with data from energies deep in MBL (E_1), phase X (E_X), NEM (E_2), and ET (E_3) [see Fig. 3(a)], we find that no phase space can be identified as phase X with a confidence over 90%. In addition, the confidence curve of phase X sharply peaks at the training energy E_X [see Fig. 3(d)]. This is in sharp contrast to the wide phase space identified as NEM with a high confidence by the three-phase classifier [see Fig. 3 (a)]. Moreover, the regime near the spectrum edge now has a lower confidence due to the confusion between MBL and X. These results indicate that the actual number of phases is less than four, and the results from the three-phase classifier suggest that there are in fact three phases: MBL, NEM, and ET.

Conclusion— We have developed a neural-network based method for determining the existence of a controversial dynamical quantum phase near many-body localization transition, which is an application of supervised machine learning beyond locating phase boundaries among existing phases. Our method allows one to detect hidden phases or conversely identify hypothetical phases that do not exist by building different neural-network classifiers. By using this technique, we have established that interacting 1D incommensurate systems with single-particle-mobility-edges may have three distinct dynamical many-body phases: the many-body localized and extended thermal phases plus the still-not-very-well-understood intermediate nonergodic metallic phase in between. Our technique is general, and should be applicable to both equilibrium and nonequilibrium quantum problems where the input training data can be obtained by calculating the entanglement spectra. We have shown that the technique is highly reliable with confidence levels for various identified phases reaching $> 99\%$ even using entanglement spectral data from systems rather modest ($L = 30$ or below) in size.

Acknowledgment. —The authors acknowledge helpful discussions with Jordan Venderley, Shenglong Xu, Xiaopeng Li, and Brian Swingle. This work is supported by Microsoft and Laboratory for Physical Sciences. The authors acknowledge the University of Maryland supercomputing resources (<http://hpcc.umd.edu>) made available for conducting the research reported in this paper.

- [2] N. Mott, *Metal-Insulator Transitions* (CRC Press, 1990).
- [3] C. M. Soukoulis and E. N. Economou, Phys. Rev. Lett. **48**, 1043 (1982).
- [4] P. A. Lee and T. V. Ramakrishnan, Rev. Mod. Phys. **57**, 287 (1985).
- [5] S. Das Sarma, A. Kobayashi, and R. E. Prange, Phys. Rev. Lett. **56**, 1280 (1986).
- [6] M. Griniasty and S. Fishman, Phys. Rev. Lett. **60**, 1334 (1988).
- [7] S. Das Sarma, S. He, and X. C. Xie, Phys. Rev. Lett. **61**, 2144 (1988).
- [8] D. J. Thouless, Phys. Rev. Lett. **61**, 2141 (1988).
- [9] S. Das Sarma, S. He, and X. C. Xie, Phys. Rev. B **41**, 5544 (1990).
- [10] J. Biddle and S. Das Sarma, Phys. Rev. Lett. **104**, 070601 (2010).
- [11] J. Biddle, D. J. Priour, B. Wang, and S. Das Sarma, Phys. Rev. B **83**, 075105 (2011).
- [12] S. Ganeshan, J. H. Pixley, and S. Das Sarma, Phys. Rev. Lett. **114**, 146601 (2015).
- [13] X. Li, X.-P. Li, and S. Das Sarma, Phys. Rev. B **96**, 085119 (2017).
- [14] H. P. Lüschen, S. Scherg, T. Kohlert, M. Schreiber, P. Bordia, X. Li, S. Das Sarma, and I. Bloch, Phys. Rev. Lett. **120**, 160404 (2018).
- [15] J. M. Deutsch, Phys. Rev. A **43**, 2046 (1991).
- [16] M. Srednicki, Phys. Rev. E **50**, 888 (1994).
- [17] I. V. Gornyi, A. D. Mirlin, and D. G. Polyakov, Phys. Rev. Lett. **95**, 206603 (2005).
- [18] D. Basko, I. Aleiner, and B. Altshuler, Ann. Phys. **321**, 1126 (2006).
- [19] V. Oganesyan and D. A. Huse, Phys. Rev. B **75**, 155111 (2007).
- [20] M. Žnidarič, T. c. v. Prosen, and P. Prelovšek, Phys. Rev. B **77**, 064426 (2008).
- [21] A. Pal and D. A. Huse, Phys. Rev. B **82**, 174411 (2010).
- [22] J. H. Bardarson, F. Pollmann, and J. E. Moore, Phys. Rev. Lett. **109**, 017202 (2012).
- [23] S. Iyer, V. Oganesyan, G. Refael, and D. A. Huse, Phys. Rev. B **87**, 134202 (2013).
- [24] R. Nandkishore and D. A. Huse, Annu. Rev. Condens. Matter Phys. **6**, 15 (2015).
- [25] R. Nandkishore, Phys. Rev. B **92**, 245141 (2015).
- [26] D. J. Luitz, N. Laflorencie, and F. Alet, Phys. Rev. B **93**, 060201 (2016).
- [27] J. Z. Imbrie, J. Stat. Phys. **163**, 998 (2016).
- [28] J. A. Kjäll, J. H. Bardarson, and F. Pollmann, Phys. Rev. Lett. **113**, 107204 (2014).
- [29] D. J. Luitz, N. Laflorencie, and F. Alet, Phys. Rev. B **91**, 081103 (2015).
- [30] I. Mondragon-Shem, A. Pal, T. L. Hughes, and C. R. Laumann, Phys. Rev. B **92**, 064203 (2015).
- [31] M. Serbyn, Z. Papić, and D. A. Abanin, Phys. Rev. X **5**, 041047 (2015).
- [32] R. Modak and S. Mukerjee, Phys. Rev. Lett. **115**, 230401 (2015).
- [33] X.-P. Li, S. Ganeshan, J. H. Pixley, and S. Das Sarma, Phys. Rev. Lett. **115**, 186601 (2015).
- [34] X.-P. Li, J. H. Pixley, D.-L. Deng, S. Ganeshan, and S. Das Sarma, Phys. Rev. B **93**, 184204 (2016).
- [35] K. Hyatt, J. R. Garrison, A. C. Potter, and B. Bauer, Phys. Rev. B **95**, 035132 (2017).
- [36] E. Baygan, S. P. Lim, and D. N. Sheng, Phys. Rev. B **92**, 195153 (2015).

* ythsu@umd.edu

† lixiao@umd.edu

[1] P. W. Anderson, Phys. Rev. **109**, 1492 (1958).

- [37] E. J. Torres-Herrera and L. F. Santos, Annalen der Physik **529**, 1600284 (2017).
- [38] D. J. Luitz, Phys. Rev. B **93**, 134201 (2016).
- [39] S. Nag and A. Garg, Phys. Rev. B **96**, 060203 (2017).
- [40] M. Schreiber, S. S. Hodgman, P. Bordia, H. P. Lüschen, M. H. Fischer, R. Vosk, E. Altman, U. Schneider, and I. Bloch, Science **349**, 842 (2015).
- [41] P. Bordia, H. P. Lüschen, S. S. Hodgman, M. Schreiber, I. Bloch, and U. Schneider, Phys. Rev. Lett. **116**, 140401 (2016).
- [42] J. y. Choi, S. Hild, J. Zeiher, P. Schauss, A. Rubio-Abadal, T. Yefsah, V. Khemani, D. A. Huse, I. Bloch, and C. Gross, Science **352**, 1547 (2016).
- [43] J. Smith, A. Lee, P. Richerme, B. Neyenhuis, P. W. Hess, P. Hauke, M. Heyl, D. A. Huse, and C. Monroe, Nat. Phys. **12**, 907 (2016).
- [44] H. Li and F. D. M. Haldane, Phys. Rev. Lett. **101**, 010504 (2008).
- [45] S. D. Geraedts, R. Nandkishore, and N. Regnault, Phys. Rev. B **93**, 174202 (2016).
- [46] F. Schindler, N. Regnault, and T. Neupert, Phys. Rev. B **95**, 245134 (2017).
- [47] J. Venderley, V. Khemani, and E.-A. Kim, ArXiv e-prints (2017), arXiv:1711.00020 [cond-mat.dis-nn].
- [48] Z.-C. Yang, C. Chamon, A. Hamma, and E. R. Mucciolo, Phys. Rev. Lett. **115**, 267206 (2015).
- [49] J. Carrasquilla and R. G. Melko, Nat. Phys. **13**, 431 (2017).
- [50] E. P. van Nieuwenburg, Y.-H. Liu, and S. D. Huber, Nat. Phys. **13**, 435 (2017).
- [51] K. Ch'ng, J. Carrasquilla, R. G. Melko, and E. Khatami, Phys. Rev. X **7**, 031038 (2017).
- [52] N. Yoshioka, Y. Akagi, and H. Katsura, arXiv:1709.05790 (2017).
- [53] G. Carleo and M. Troyer, Science **355**, 602 (2017).
- [54] D.-L. Deng, X. Li, and S. Das Sarma, Phys. Rev. B **96**, 195145 (2017).
- [55] L. Wang, Phys. Rev. B **94**, 195105 (2016).
- [56] L.-F. Arsenault, O. A. von Lilienfeld, and A. J. Millis, arXiv:1506.08858 (2015).
- [57] D.-L. Deng, X. Li, and S. Das Sarma, Phys. Rev. X **7**, 021021 (2017).
- [58] S. J. Wetzel, Phys. Rev. E **96**, 022140 (2017).
- [59] W. Hu, R. R. P. Singh, and R. T. Scalettar, Phys. Rev. E **95**, 062122 (2017).
- [60] X. Gao and L.-M. Duan, Nat. Commu. , 662 (2017).
- [61] Y. Huang and J. E. Moore, arXiv:1701.06246 (2017).
- [62] J. Chen, S. Cheng, H. Xie, L. Wang, and T. Xiang, Phys. Rev. B **97**, 085104 (2018).
- [63] Z. Cai and J. Liu, Phys. Rev. B **97**, 035116 (2018).
- [64] F. Schindler, N. Regnault, and T. Neupert, Phys. Rev. B **95**, 245134 (2017).
- [65] P. Broecker, F. F. Assaad, and S. Trebst, arXiv:1707.00663 (2017).
- [66] Y. Nomura, A. S. Darmawan, Y. Yamaji, and M. Imada, Phys. Rev. B **96**, 205152 (2017).
- [67] Y. Zhang and E.-A. Kim, Phys. Rev. Lett. **118**, 216401 (2017).
- [68] P. Broecker, J. Carrasquilla, R. G. Melko, and S. Trebst, Sci. Rep. **7**, 8823 (2017).
- [69] Y. LeCun and C. Cortes, (2010).
- [70] S. Aubry and G. André, Ann. Israel Phys. Soc **3**, 18 (1980).